Beyond Condensed Matter Physics on the Nanoscale: The Role of Ionic and Electrochemical Phenomena in the Physical Functionalities of Oxide Materials

Sergei V. Kalinin,[†,*] Albina Borisevich,[‡,*] and Dillon Fong[§,*]

[†]The Center for Nanophase Materials Sciences and [‡]Materials Sciences and Technology Division, Oak Ridge National Laboratory, Oak Ridge, Tennessee 37831, United States, and [§]Materials Science Division, Argonne National Laboratory, Argonne, Illinois 60439, United States

ABSTRACT Novel physical functionality enabled by nanoscale control of materials has been the target of intense scientific exploration and interest for the last two decades, leading directly to the explosive growth of nanoscience and nanotechnology. However, this transition to nanometer scales also blurs the boundary between classical physical and electrochemical phenomena, due to smaller transport lengths, larger chemical and electrostatic potential gradients, and higher surface/volume ratios. While well-recognized for many decades in areas such as ferroelectricity, these phenomena remained largely outside the realm of condensed matter physics studies. Here, we offer a perspective on the role of electrochemical phenomena in the nanoscale physics of correlated oxides and summarize the challenges for local characterization of these behaviors.

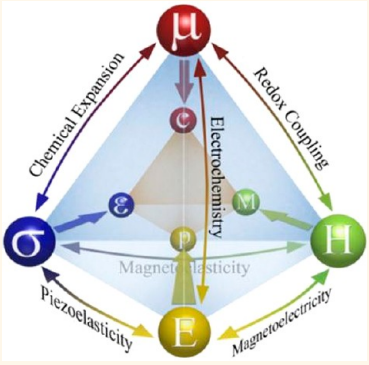

The rapid development of condensed matter physics and materials science in the last century has furnished mankind with a deep understanding of the laws and paradigms that control nature around us, with such areas as semiconductor and quantum physics, magnetism, optics, and ferroelectricity all becoming open for exploration. Many of these areas evolved from conceptual discoveries to real world devices and applications, with the field of semiconductors arguably having the most impact, having given rise to modern information technologies, lasers that enabled modern communications, and nuclear magnetic resonance in medicine, to name but a few.[1] Some areas, such as quantum computing[2,3] and spintronics,[4,5] are presently developing from the concept to the prototype stage. As for the others, early phenomenological discoveries have led to decades of fundamental research, with such prominent examples as the physics of disordered magnetics and ferroelectrics.[6] Together, advances in materials synthesis, characterization, and theory have established this gamut of scientific disciplines that now underpin modern technical civilization.

The more recent hallmark of our time is the explosive growth in nanoscience and nanotechnology. While the conceptual framework for the field was outlined by R. Feynman in his celebrated lecture "There is plenty of room at the bottom", it was the development of readily available benchtop instrumentation, most notably scanning probe and electron microscopies, that enabled rapid experimental progress in multiple laboratories worldwide.[7] According to the programmatic documents for the national nanotechnology initiative, "nano" is defined as novel structural, optical, magnetic, and electronic properties induced by atter confinement.[8] The interface between the nano- and physical sciences has spawned or reinvigorated multiple areas of research, including the physics of heterophase boundaries, tunneling barriers, quantum electronics, and nanocarbon. However, in many of these areas, it is typically understood that nanoscale

* Address correspondence to sergei2@ornl.gov, albinab@ornl.gov, fong@anl.gov.

Published online December 03, 2012
10.1021/nn304930x

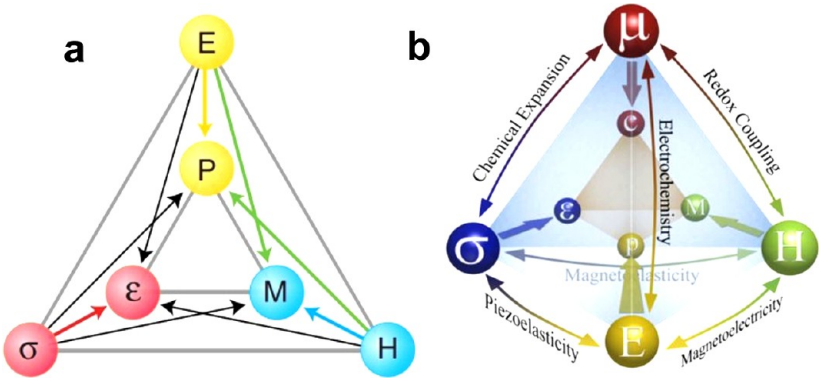

Figure 1. (a) Fiebig−Spaldin diagram showing the interrelationship of electric field *E*, magnetic field *H*, and stress σ controlling the electric polarization *P*, magnetization *M*, and strain ε, in multiferroics.[18] Reprinted with permission from ref 18. Copyright 2005 American Association for the Advancement of Science. (b) Physics of multiferroics can change dramatically when mobile ionic species are considered, which adds a new dimension to the physics. Here, μ is chemical potential and *c* is concentration. The base of the tetrahedron in (b) is equivalent to (a).[19] Reprinted with permission from ref 19. Copyright 2012 Cambridge University Press.

phenomena will affect the *physical* properties of matter, for example, through changes in bonding and minute distortions from ideal positions that constitute order parameter fields, charge carrier distributions that couple to magnetic and semiconducting properties, confinement effects on electronic structure, and so on. The implicit assumption is that the matter itself, that is, the number and connectivity of atoms, is *constant* during the manifestation of physical property.

However, a prominent aspect of nanoscale systems is that the constraints on chemical invariance that are well-defined for macroscopic systems are relaxed in nanoscale systems, blurring the boundary between physical and (electro)chemical phenomena. This overlap is particularly pronounced in the field of correlated oxides. These materials have remained on the forefront of physical research for the past 25 years,[9,10] and oxides, like the manganites with giant magnetoresistance and phase separation, cobaltites with intricate high-low spin transitions, ferrites, nickelates, and others are the same materials that have been explored for decades in solid oxide fuel cell (SOFC) applications.[11−13] Solid-state electrochemists are often more focused on chemical and ionic transport behavior, including the parameters defining gas−solid reactions, vacancy transport and ordering, and coupling between ionic and electronic electrochemical potentials, than on the particular physics of the system.[14,15] There are notable exceptions, of course, such as the pioneering work of Mitchell *et al.*, who demonstrated that during the growth of $La_{1-x}Sr_xMnO_3$ crystals, just a four-order change of magnitude in the oxygen partial pressure has as large of an effect on the structures grown, as does changing the doping level by 30%.[16] Furthermore, oxygen nonstoichiometry is known to play a critical role in the superconductivity of many cuprates, such as $La_2CuO_{4+\delta}$.[17] However, this conceptual boundary between electrochemical and physical studies is often justified. Solid oxide fuel cells operate at the temperatures well above 500 °C, where both oxygen reduction/evolution reactions and ionic transport are enabled, whereas most physical studies are performed at low temperatures, where quantum phenomena can be explored.

However, the situation changes dramatically with nanoscale systems. Indeed, SOFC operation implies current densities on the order of 1 A/cm^2 through 10−100 μm of material (cathode, electrolyte, anode) under (chemical) driving forces of ~1 eV. In comparison, scanning probe microscopy measurements (*e.g.*, conductive AFM) or the operation of tunneling barriers typically imply biases of 1−10 V, often applied across a few nanometers of material. Even static objects such as ferroelectric domain walls or oxide−oxide interfaces will be associated with significant electrochemical potential gradients. Unlike SOFCs, significant changes in physical properties can be expected even if only a small number of vacancies (*e.g.*, ~0.1/unit cell) migrate on the time scale of days at room temperature and below. Simple estimates of diffusional mobilities suggest that this is entirely possible.

The obvious question is whether the ionic motion can affect physical functionalities. In this respect, it is instructive to consider the famed Fiebig−Spaldin diagram[18] shown in Figure 1a, which illustrates the primary manifestations of multiferroic behavior and is directly tied to the resurgence of this field (primarily for oxide materials) in the last several years. For systems with a varying number of ionic species, it is necessary to add an additional chemical degree of freedom—for example, the concentration of oxygen vacancies. Notably, the couplings between chemical and physical functionalities will often be much stronger than those between physical functionalities *per se*. For example, while bias-induced strains in ferroelectrics and multiferroics ($P-\sigma$ coupling) rarely exceed fractions of 1%, chemical strains can be readily manifested on the 3−30% levels and even higher for phase change processes.

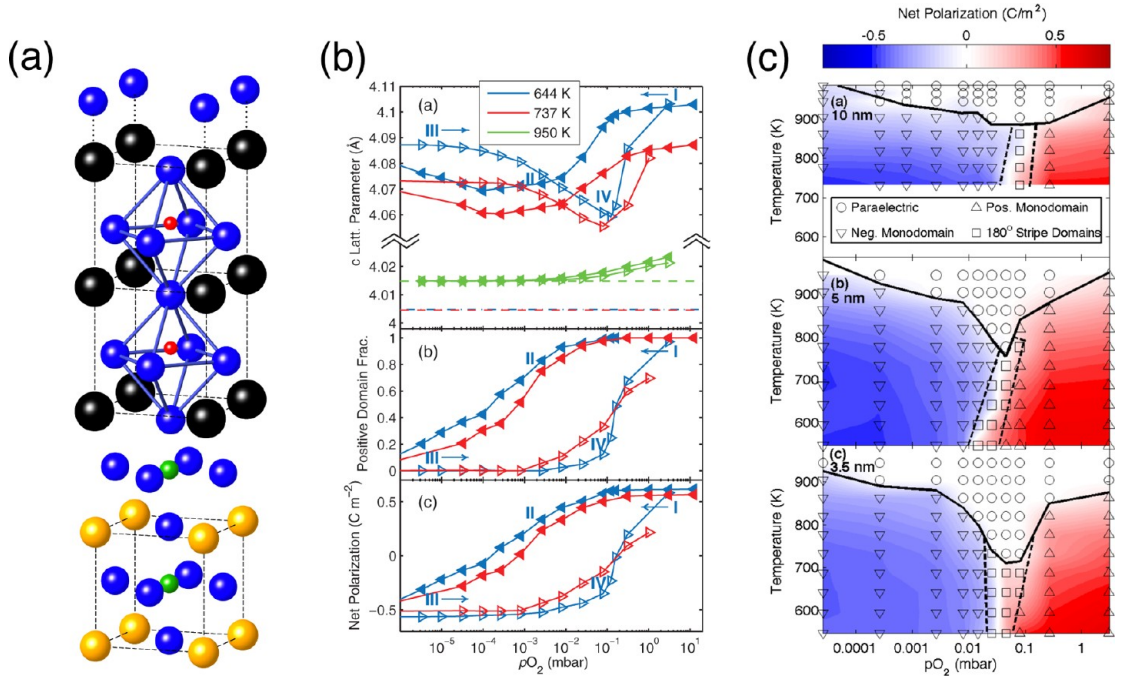

Figure 2. (a) Structure for oxygen adsorption on $PbTiO_3/SrRuO_3$. (b) Results from a 10 nm $PbTiO_3/SrRuO_3$ heterostructure, showing responses to changes in oxygen partial pressure. Reprinted with permission from ref 25. Copyright 2009 American Physical Society. (c) Measured temperature−oxygen partial pressure diagrams for $PbTiO_3/SrRuO_3$ heterostructures with three different $PbTiO_3$ thicknesses.[34] Reprinted with permission from ref 34. Copyright 2011 American Physical Society.

The interesting corollary to this is that, unlike electronic carriers, vacancies effectively couple to the molar volume of material and hence open an effective channel for strain relaxation in inhomogeneous systems. Hence, bias−strain coupling mediated by ionic transport will (for systems with mobile ions) be expected to be much stronger than direct piezoelectric or electrostrictive effects. Similarly, changes in the redox state of metal cation will significantly affect the magnetic properties of a system, and so on.

Given the obvious impact of oxygen vacancies on the physics of transition metal oxides, the natural questions are: how do we probe these effects experimentally and theoretically, and can such effects can be harnessed for applications? In answering these questions, it is pertinent to note that electrochemical effects on functionality are often observed *indirectly*, and direct probing of the oxygen vacancy concentration or the stoichiometry in general on the mesoscopic and atomic levels remains elusive. In this Perspective, we provide an overview of electrochemical effects in the physics of oxides, describe strategies used to study them, and discuss how such knowledge can affect future scientific development.

In this Perspective, we provide an overview of electrochemical effects in the physics of oxides, describe strategies used to study them, and discuss how such knowledge can affect future scientific development.

Indirect Evidence for Electrochemical Phenomena in the Physics of Oxides. An early example in which the importance of (surface) electrochemical phenomena was recognized is ferroelectricity. A ferroelectric is a material that can exhibit nonzero bulk polarization and can be switched between two or more equivalent states by an external electric field.[20] The presence of nonzero polarization, **P**, in the bulk necessarily implies the presence of nonzero polarization charge, $\sigma = \mathbf{P}\cdot\mathbf{n}$, where **n** is the normal vector, at surfaces and interfaces. Remarkably, the free energy associated with uncompensated polarization charge scales as the cube of system size, L^3 (similar to bulk terms), as opposed to L^2 scaling for classical surface terms. These depolarization field effects were predicted to destabilize the polar phase in ferroelectrics, leading to obvious contradictions with the experimental observations. To resolve this paradox, it was postulated that polarization charges are screened, that is, compensated by extraneous charges with screening lengths much smaller than L. Under the influence of semiconductor theory, the field of ferroelectric semiconductors has emerged, analyzing the interplay between band bending and polarization phenomena.[21] Interestingly, while it was realized early on that polarization charge can be also compensated by surface electrochemical processes (*e.g.*, the

adsorption of charged ions), few systematic theoretical or experimental studies were undertaken.

The situation changed dramatically in the past decade, spurred on by advances in surface-sensitive scattering techniques, scanning probe microscopy, and first-principles theory. Notably, the presence of polar adsorbates on oxide surfaces[22−24] and their coupling to ferroelectric stability[25−27] and polarization dynamics[28−32] are now well-recognized, providing a broader context for this model. In 2006, it was shown that for the prototypical ferroelectric material $PbTiO_3$, ionic adsorbates could stabilize the monodomain polarization state.[26] In 2009, the same group from Argonne National Laboratory demonstrated that varying the composition of the gaseous environment could be used to switch the polarization direction.[25] Specifically, epitaxial $PbTiO_3$ films grown on conducting $SrRuO_3$ were uniformly polarized in the positive direction (along the surface normal) after growth of the film by metal−organic chemical vapor deposition (MOCVD). This result was in sharp contrast to films grown directly on insulating $SrTiO_3$, which exhibited 180° stripe domains.[33] The observation of positive polarization suggested the existence of a layer of negative screening charge at the $PbTiO_3$ surface. This layer could originate from any number of species in the MOCVD environment, but density functional theory (DFT) calculations suggested that the likely ion was oxygen, bonded to Pb in the topmost PbO surface, as shown in Figure 2a. The importance of oxygen was elucidated in the 2009 study, where it was observed that high oxygen partial pressures led to positive polarization and low oxygen partial pressures led to negative polarization. The polarization change was found to be reversible, enabling construction of the well-known butterfly and hysteresis loops, not as a function of applied field but rather of oxygen partial pressure, as shown in Figure 2b. A natural assumption is that, since an oxygen ion can screen the positive polarization, the loss of oxygen can screen the negative polarization. This is consistent with the observation of a (4×1) surface reconstruction in the low oxygen partial pressure condition:[25] one oxygen vacancy per four surface unit cells would provide sufficient compensating charge for the magnitude of the observed $PbTiO_3$ polarization. According to the DFT results, a perfectly stoichiometric surface favors the nonpolar state.

A more recent publication demonstrated that, at intermediate oxygen partial pressures, the $PbTiO_3$ film cannot stabilize a monodomain state and must either remain paraelectric or form stripe domains, depending on the temperature (Figure 2c).[34] At sufficiently high temperatures, this leads to the interesting phenomenon of ferroelectric switching without domain formation,[35] which has only been observed with an ionic compensation mechanism. As discussed by Highland and colleagues,[34,36] if simple Langmuir adsorption/desorption of doubly charged oxygen ions is incorporated into a ferroelectric polarization model based on Landau−Ginzburg−Devonshire theory, one can calculate a polarization phase diagram similar to one the shown in Figure 2c.

In parallel, strong evidence in favor of ionic compensation was obtained in the context of scanning probe microscopy (SPM) studies of ferroelectric domains by Kelvin probe force microscopy (or scanning surface potential microscopy). Studies by Kalinin and Bonnell, motivated by the observation of ferroelectric domains and phase transitions, demonstrated a unexpected increase of domain-related potentials (preserving relative signs) above the ferroelectric phase transition with subsequent slow relaxation,[23,37] behavior that can be understood only by postulating screening of polarization charges by adsorbed ionic species.[38] A complementary result was the observation of temperature-induced domain potential inversion upon cooling,[39] an effect enabled by the momentary increase of polarization charge compared to the screening charge. Similar behaviors were observed at grain boundaries in oxides,[40] during tip-induced electrification of (nominally conductive) oxide surfaces,[22,24] and in lateral bias experiments on oxide surfaces,[41] pointing to the ubiquitous presence of ionic screening charges.

Notably, the effects linked to surface charge dynamics can strongly affect other measurements. For example, applications in ferroelectric data storage have motivated a number of experimental studies of tip-induced domain dynamics,[42,43] as well as the development of associated thermodynamic and kinetic theories, typically in the context of purely physical models. However, studies of phenomena such as back-switching[32] have hinted at possible surface compensation mechanisms, and recent studies of humidity and atmospheric effects[30,44] on tip-induced domain dynamics provide strong evidence of ionic screening, in agreement with the thermodynamic analysis by Morozovska.[45] Overall, polarization switching for oxide surfaces in the presence of water layers is probably best described as a physical polarization switching process coupled to the surface electrochemical process of dissociative water adsorption. Similarly, domain growth in the tip field can be controlled by the lateral spreading of charged ionic species injected at the tip−surface junction. Elucidation of the relative contributions of physical and electrochemical processes will be required for future progress.

Given the important role surface electrochemistry plays in ferroelectrics, it is natural to assume that it will be significant for other (non-switchable) polar systems. A paradigmatic example is the $LaAlO_3$−$SrTiO_3$ (LAO−STO) system renowned for the two-dimensional electron gas (2DEG) at its interface, unique magnetotransport and superconductive properties, and amenability to local control (charge writing). The unique

physical properties of LAO–STO were originally interpreted in the context of polar catastrophe,[46] that is, the transfer of surface electrons to the interface at a certain critical thickness and the formation of an interface charge layer. The alternative mechanism for 2DEG formation is *chemical* cationic intermixing at the interfaces, that is, the formation of metallic La-doped $SrTiO_3$.[47–49] Finally, a number of authors consider the formation of oxygen vacancies[50–54] on the LAO surface or segregation from the bulk as integral to the process. Recently, a number of experimental studies have elucidated the role of charged surface adsorbates (water cycle mechanisms) on LAO–STO switching.[55–60] A theoretical effort by Bristowe *et al.*[61] analyzed the dynamic formation of *surface* vacancies as a mechanism for charge writing and formation of the 2DEG in LAO–STO.

Here, we briefly comment on bulk electrochemical phenomena in the physics of nanoscale systems. These phenomena were long explored in the context of ferroelectric fatigue[62,63] and, more recently, ionic transport in ferroelectrics. However, more widespread attention to these phenomena has been stimulated by recent advances in electroresistive systems, following the seminal work of Strukov.[64] Electroresistance in a very broad range of materials, including TiO_2 and the titanates, NiO, Nb_2O_5, HfO_2, and many others, is invariably linked to field-induced ion dynamics and solid-state electrochemical processes.[65–68] Depending on the specific aspects of the system, these transformation fronts can be either uniform or unstable, thus giving rise to filamentary switching phenomena. Recently, extensive studies of these phenomena were reported in the context of resistive switching in transition metal oxides such as $SrTiO_3$[69] and $BiFeO_3$.[70] Notably, the electric fields involved in resistive switching are very close to those reported for ferroelectric tunneling barriers. While the ultimate mechanisms can be resolved only with atomically resolved scattering and electron microscopy studies, these estimates suggest that electrochemical mechanisms should be considered when interpreting results. Furthermore, more complex couplings are possible.[71]

Finally, nontrivial electrochemical effects can occur at internal interfaces such as ferroelectric and ferroelastic domain walls. This has been explored theoretically since the 1960s,[72,73] but advances in SPM now permit direct experimental probing of the physical properties of a single wall. The discovery of enhanced domain wall conductivity by Seidel *et al.*[74] has stimulated extensive theoretical efforts, which have enabled the identification of multiple causes for interfacial conductivity, including symmetry-induced band gap reduction,[75] carrier segregation,[76–78] and so forth. However, observations such as conductance hysteresis at ferroelectric domain walls[79] and one-dimensional vortex/antivortex cores[80] have demonstrated the importance of slow polarization dynamics and oxygen vacancy segregation.[81,82] These studies indicate that oxygen vacancies play significant roles in wall conductivity. Furthermore, they provide numerous examples of hysteretic and memory effects that cannot be explained by a simple picture of static wall conductance but are fully consistent with the concept of dynamic wall conductance and vacancy accumulation.

There are many other examples of the (discovered) role of surface and near-surface electrochemical processes, such as piezoresistance in silicon nanowires[83] and hysteresis in carbon nanotube transistors[84,85] and graphene[86,87] transistors. Researchers have also shown that the electrical double layer at the interface between an oxide surface and an ionic or polar liquid can be used to induce electronic phase transitions,[88,89] and Xie *et al.* demonstrated that polar adsorbates at the $LaAlO_3$ surface can be used to control the conductivity of the LAO–STO interface buried several nanometers below.[90] Recent work by Cheong[70] and Skowronski[69] suggests that vacancy redistribution in oxides is possible even at room temperature and below in sufficiently strong electric fields. Overall, the examples above suggest that electrochemical effects play a large, if not readily verifiable, role in physical behaviors on the nanoscale. Whenever significant time effects, hysteresis, and abnormally strong couplings are observed, and if the nature of the systems allows for possible electrochemistry, these mechanisms should definitely be considered along with more classical physics-based interpretations.

What We Want To Know. The multiple examples of electrochemical phenomena in solids and surfaces/interfaces raise the obvious question of why these phenomena have not been explored more. One possible argument is that the importance of point defects in these materials (other than growth impurities) has not been fully recognized, particularly by those focused on ground-state behavior. However, the second, and probably more important, answer is that these (electro)-chemical degrees of freedom are exceedingly difficult to control—often the presence and character of surface species, defect concentrations, and other vital parameters are difficult to access experimentally. Obviously, both *static* defect distributions as well as their *dynamics* during physical measurements are relevant. Whereas at macroscopic scales these phenomena are amenable to classical electrochemical methods,[91,92] this is not the case for nanoscale systems. Below, we attempt to summarize the potential of current experimental methods to explore these phenomena locally.

Scanning Probe Microscopy. Much of the progress in chemistry, surface science, catalysis, and solid-state physics in the last two decades is related to development of scanning probe methods.[7] In areas where quantitative measurements are possible, new scientific areas have emerged,

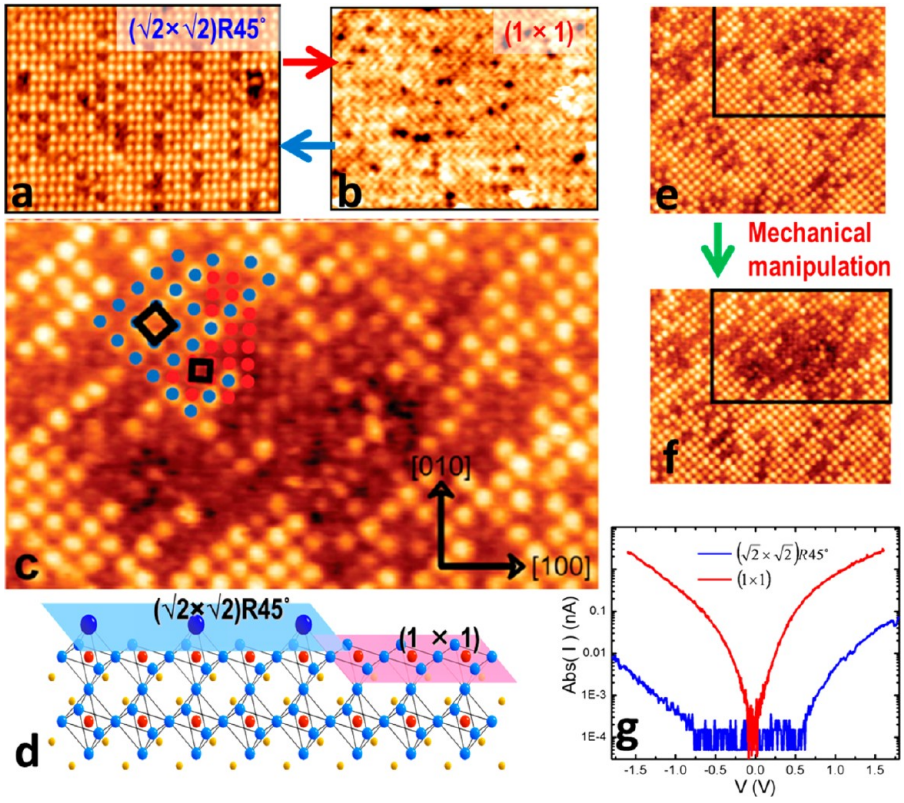

Figure 3. Scanning tunneling microscopy (STM) imaging and spectroscopy of $La_{5/8}Ca_{3/8}MnO_3$ surfaces. The surface shows two main structures ($\sqrt{2} \times \sqrt{2})R45°$ (a) and (1 × 1) (b) depending on the experimental conditions. The correlations and the unit cells of the two structures are marked in (c) with blue dots for $(\sqrt{2} \times \sqrt{2})R45°$ and red dots for (1 × 1). (d) Side view of the stick and ball models for the two structures, with red, large blue, and small blue balls representing Mn, O atoms located atop the MnO_6 octahedra, and O at the MnO_6 layer, respectively. (e,f) Exact same position before and after mechanical scratch with a STM tip. (g) Scanning tunneling spectroscopy (STS) current−voltage (*I*−*V*) curves obtained from the two structures. Image sizes are (a,b) 16 nm × 12 nm; (c) 13 nm × 8 nm; (e,f) 18 nm × 18 nm. Reprinted with permission from ref 98. Copyright 2009 American Physical Society.

most prominently molecular unfolding spectroscopy for studying the kinetics and thermodynamics of single-molecule reactions[93] and piezoresponse force microscopy and spectroscopy of ferroelectrics.[94−96] By comparison, in areas such as nanomechanics, where quantitative noninvasive measurements by SPM are hindered by topographic effects, progress has been markedly slower as compared with nanoindentation-based techniques[97] that allow quantitative measurements, albeit at larger scales. The other important areas of SPM applications are those that enable atomic-resolution imaging, in which case even semiquantitative data are sufficient to gain a deep understanding of the atomic and electronic structure of surfaces.

Notably, the vast majority of SPM methods are near-field in nature—meaning that the signal generation volume is centered at a tip−surface junction and the penetration depth is commensurate with lateral resolution. In other words, if the lateral resolution of a ferroelectric domain wall as seen by piezoresponse force microscopy is ~30 nm, the electric field penetration depth in the material is ~15 nm (depending on the dielectric anisotropy). Similarly, if scanning tunneling microscopy (STM) images surface with atomic resolution, the signals are dominated by the top 1−2 atomic layers.

> **Much of the progress in chemistry, surface science, catalysis, and solid-state physics in the last two decades is related to development of scanning probe methods.**

We now consider the feasibility of SPM studies of vacancy dynamics. On the atomic level, the observability of vacancies requires stable surfaces that are static (*i.e.*, extant vacancies should be stable during imaging). A beautiful example of such work is illustrated in Figure 3.[98] Here, a $La_{5/8}Ca_{3/8}MnO_3(001)$ (LCMO) thin film was grown using pulsed laser deposition (PLD) and transferred *in situ* to the STM chamber. The atomically resolved imaging allows observation of the $(\sqrt{2} \times \sqrt{2})R45°$ reconstruction formed by oxygen atoms and vacancies in a checkerboard pattern. Annealing of the surface at low oxygen partial pressure yields the reduced 1 × 1 surface, while at

higher pressures, a 2 × 2 and other, more complex reconstructions are observed. Interestingly, scanning with a STM tip can also remove oxygen adatoms. Most remarkably, this process is associated with a metal−insulator transition of the surface in the area with injected vacancies, as can be seen from STM current−voltage (*I*−*V*) curves in Figure 3.

This study illustrates several complementary concepts. For the solid-state electrochemist, this is direct observation of oxygen vacancies on a manganite surface, which are directly responsible for the oxygen reduction/evolution reactions that underpin SOFC functionality,[11] and hence represents a pathway to study vacancies at the atomic level. For the electrical engineer, this is a demonstration of electroresistive switching at the nanometer scale, illustrating the ultimate scalability limits of these devices. For physicists, this is an illustration of the role of local oxygen stoichiometry on physical properties. One can only speculate what the full implications of these studies may be. For example, if mechanical manipulation by the tip can change the local stoichiometry and couple to the metal−insulator transition and, at the same time, oxygen stoichiometry affects polarization (Figure 2), it is conceivable that tip manipulation of oxygen atoms in a mesoscopic experiment can cause ferroelectric switching (as was observed recently[99]).

Despite the spectacular potential of such studies, these experiments are extremely time-consuming. Suffice it to say that atomically resolved imaging of *in situ* PLD-grown oxide surfaces was achieved only in a limited number of cases,[98,100−102] whereas classical surface preparation techniques are applicable only for a limited number of oxides (most notably the titanates). Second, atomic-resolution imaging requires vacancies to be static, necessitating temperatures well below the operation regimes of SOFCs and where relevant materials properties, reaction mechanisms, and physical behavior can differ significantly from those relevant to ionic functionality.

An alternative approach for probing vacancy-controlled behaviors can be based on mesoscopic SPMs that are sensitive to vacancy flows (much like STM is sensitive to electronic flow), bringing forth the challenge of ionic current measurements on the nanoscale. Traditional electrochemical detection methods rely on conversion between ionic and electronic currents and are difficult to scale directly to the nanometer level due to the large ionic impedances and the presence of stray electronic currents. An alternative solution is the detection of strains in a material induced by changes in vacancy concentration (Vegard strains), a technique referred to as electrochemical strain microscopy (ESM).[19,103−105] Simple estimates suggest that this approach enables probing electrochemical response on the nanometer scale, many orders of magnitude below classical electrochemical strategies.[106,107] Notably, measured strain responses in ESM are directly proportional to the number of transferred ions, thus providing information similar to classical electrochemical strategies.

Electron Microscopy: Electronic Spectroscopy, Ordering, Expansivity. After the implementation of aberration correction in electron microscopy, characterization of the atomic and electronic structure of the materials became possible at an unprecedented level of detail. Single atoms can now be detected and identified *via* imaging[108] and spectroscopy, both by electron energy loss spectroscopy (EELS)[109] and energy-dispersive X-ray spectroscopy (EDX).[110] Using EELS fine structure analysis, changes in oxidation states and coordination environments of the elements can be tracked column by column in materials as diverse as stripe-ordered manganites,[111] other mixed valence compounds,[112] and layered oxides.[113,114] Increased signal-to-noise in the images has also enabled unit-cell by unit-cell studies of structural distortions, thus permitting the mapping of order parameters such as strain,[115−117] polarization,[116,118−121] and octahedral tilts[117,122,123] with atomic-scale resolution. Notably, these observations rely on the quantitative interpretation of the image of the primary lattice, whether it is a direct measurement of spacings or a specific deviation from some ideal model. Direct imaging and quantification of oxygen vacancies, which generate no primary signals of their own, are necessarily more challenging.

Oxygen vacancies can be tracked indirectly by examining local composition and oxidation states as reflected in the fine structure of the EELS edges of oxygen and the surrounding cations or the overall intensity of the oxygen K EELS edge.[124−127] These results can be interpreted in conjunction with the available structural and theoretical information about the studied system to reveal evidence of nanometer-scale electrochemical phenomena. For example, in work by Cantoni *et al.*,[128] the strain distribution around $BaZrO_3$ (BZO) nanocolumns in the matrix of the superconductor rare-earth $REBa_2Cu_3O_{7-\delta}$ (REBCO) was investigated. Figure 4a shows the overall view of the interface of one BZO inclusion, with copper planes/chains in REBCO ordering along the direction parallel to the interface. From the image, it was possible to quantify the in-plane lattice parameter and, hence, strain, as a function of the distance from the interface. However, the observed profile diverged considerably from the one expected theoretically (Figure 4b), such that predicted high strains close to the interface were not observed. From EELS studies of the interface, it became apparent that the region immediately adjacent to the interface contained lower oxygen concentrations (Figure 4c, note alignment with Figure 4b). Therefore, in this system, oxygen vacancies are injected into the near-interface region to alleviate excess strain, exemplifying a process occurring along the $\sigma-\mu$ axis of the tetrahedron in Figure 1b.

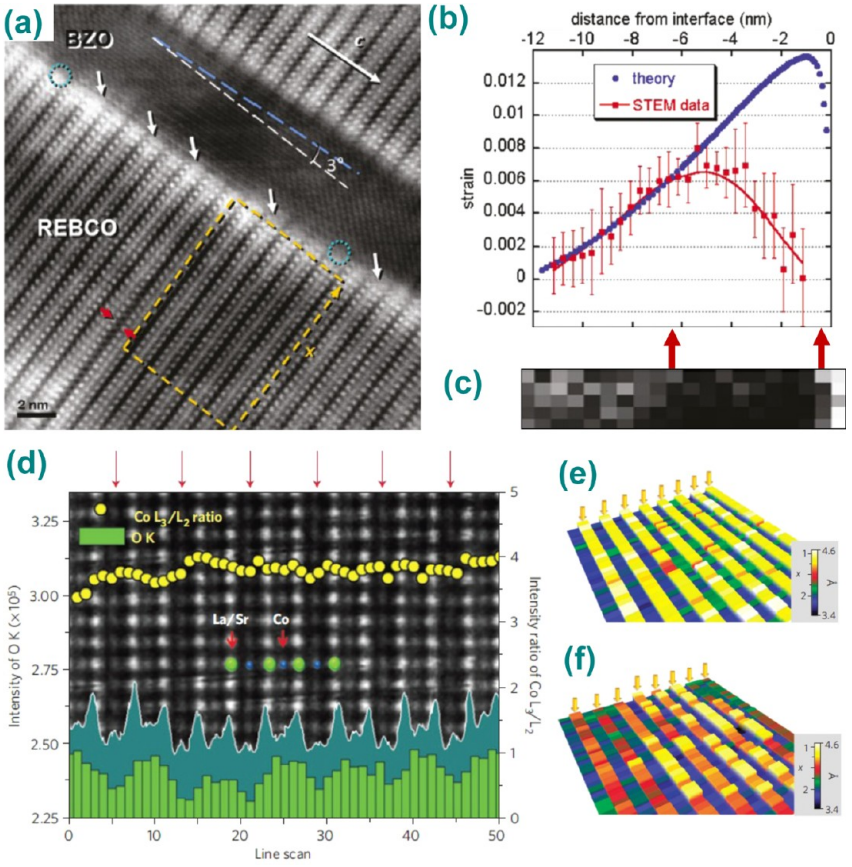

Figure 4. Oxygen vacancy studies by electron microscopy. (a) High-resolution *Z*-contrast STEM image of the sectioned BZO nanocolumn in superconducting REBCO matrix; (b) comparison between analytically calculated strain (blue dots) and experimentally derived strain (red squares); the experimental strain is obtained from interatomic distances within the yellow box in (a). (c) Integrated intensity profile of O−K EELS edge across the same region as (b), given on the same scale; red arrows highlight correspondence of the oxygen-depleted region to the region of decreased strain. (d) HAADF image of a vacancy-ordered LSCO film, with overlapping HAADF profile (teal) and oxygen K EELS edge intensity profile (green); oxygen-depleted planes are highlighted with arrows. (e,f) Lattice spacing/local oxygen concentration maps for (e) LSCO/NGO and (f) LSCO/LSAT films, illustrating differences in overall oxygen concentration and local degree of disorder. Adapted with permission from refs 128 (a−c) and 141 (d−f). Copyrights 2011 American Chemical Society and 2012 Nature Publishing Group, respectively.

Progress in spectroscopic techniques notwithstanding, possible imaging-based methods for oxygen vacancy detection are still being relentlessly pursued. For example, the feasibility of local vacancy concentration measurements *via* matching the observed intensities to high-resolution transmission electron microscopy (HRTEM) simulations was demonstrated for $BaTiO_3$ grain boundaries.[129] Other researchers have pointed out correlations between the low-angle annular dark-field image signal and signatures of oxygen vacancies in the EELS fine structure in reduced $SrTiO_3$, thus suggesting the former as a visual vacancy detection tool.[130] However, neither of these approaches has yet proven sufficiently general to develop into a quantitative tool. Tantalizingly, in some systems, notably nonstoichiometric perovskites and brownmillerites where oxygen vacancies order in the alternating [001] pseudocubic planes,[131] ordering is manifested as image contrast in high-angle annular dark-field (HAADF) images, such that oxygen-poor planes appear darker than those that are more oxygenated.[132−136] Using high-resolution HAADF imaging and theoretical simulations for the $(La,Sr)CoO_{3-x}$ system, this effect was demonstrated to result from the combination of the increased Debye−Waller factors of the cations in the oxygen-depleted layers and lattice expansion caused by vacancy accumulation.[132] The latter phenomenon deserves further exploration.

Progress in spectroscopic techniques notwithstanding, possible imaging-based methods for oxygen vacancy detection are still being relentlessly pursued.

Chemical expansivity is well-known in the field of solid-state ionics, as exemplified by the expansion of most oxygen-conducting materials in a reducing atmosphere.[137−139]

The expansion can be detected by dilatometric methods (see, *e.g.*, refs 138 and 140), with expansion scaling linearly with respect to the log of oxygen partial pressure. In work by Kim *et al.*,[141] the chemical expansivity concept was extended to the atomic level, demonstrating that the local lattice spacing measured from HAADF images can be directly connected to the local oxygen concentration. The study evaluated two $(La_{0.5}Sr_{0.5})CoO_{3-x}$ (LSCO) thin films grown under the same conditions on different substrates with very similar lattice parameters but different tilts: $(La,Sr)(Al,Ta)O_3$ (LSAT) (the $a^0a^0a^0$ Glazer tilt system) and $NdGaO_3$ (NGO) (the $a^-a^-c^+$ system).[142] Both films showed lattice parameter modulations; EELS studies showed that the modulations were associated with oxygen vacancy ordering (Figure 4d) such that the integrated intensity of the oxygen edge decreased for the darker CoO_{2-x} planes. Detailed structural studies demonstrated that the LSCO/NGO film had the composition $(La_{0.5}Sr_{0.5})CoO_{2.5}$. The LSCO film grown on LSAT exhibited smaller lattice expansion. First-principles calculations showed that, for this system, the spacing of the depleted CoO_{2-x} layer increases linearly as more vacancies are injected; the theoretical dependence, which agreed with experimental measurements for CoO and CoO_2 layer compositions, was then used as a calibration curve to translate lattice spacings into local oxygen content (Figure 4e,f). The average composition for the film grown on the LSAT substrate was determined to be $(La_{0.5}Sr_{0.5})CoO_{2.75}$, and its vacancy distribution was more inhomogeneous, highlighting the sensitivity of the method to both absolute changes and relative disorder. Interestingly, in this study, a subtle structural effect (different octahedral tilts in the substrate) produced major changes in film *composition*, highlighting the fact that oxygen vacancies are intimately connected to all structural and physical aspects of the oxide materials.

Note that a similar approach—interpreting structural signals as evidence for the presence of vacancies by employing first-principles calculations—can also be used for specific oxide interfaces, where vacancies can affect not only lattice spacings but also polar cation displacements.[143,144] It has also been suggested that oxygen vacancy behavior can be described by mesoscopic theories similar to those developed for ferroic materials, and local studies of defects can help find gradient terms for free energy expansions that are not available from bulk measurements.[71] Theoretical models of this sort are especially important for systems where multiple physical and chemical processes are occurring at the same time, such as polar oxide interfaces. For example, it was demonstrated by Cantoni *et al.*[145] that careful analysis of the structural and EELS information at the LAO–STO interface allows the unambiguous separation of three different contributors to interface behavior, namely, cation polarization by interface charge, cation interdiffusion, and oxygen vacancy injection.

X-ray Methods: Scattering and Spectroscopy. Much like for the electron microscopy studies described above, the sub-angstrom resolution of X-ray scattering can provide information on relative oxygen vacancy concentrations. Furthermore, with *in situ* X-ray scattering, changes in oxygen vacancy concentrations can be probed dynamically. However, it should be noted that the degree of expansivity varies considerably among the different oxides (*e.g.*, it is negligible for $SrTiO_3$).[146,147] In nanoscale systems, the oxygen vacancies tend to couple with strain and interact with phase boundaries. As shown by Donner *et al.*,[148] epitaxial strain in $La_{0.5}Sr_{0.5}CoO_{3-\delta}$ thin films can lower the oxygen vacancy formation energy, thus promoting higher vacancy concentrations and vacancy ordering. Furthermore, nanoscale structures allow short equilibration times such that vacancies can quickly move from one phase to another. This can occur even during the growth process. For example, using *in situ* X-ray scattering during PLD, Ferguson *et al.*[149] found that, after reaching a critical thickness, the vacancies present in an oxygen-deficient overlayer of $SrTiO_{3-\delta}$ migrate to the underlying $La_{0.7}Sr_{0.3}MnO_3$ layer, causing the formation of the oxygen-vacancy-ordered brownmillerite phase. It should be emphasized that the use of techniques that allow direct measurement of the lattice response while varying the oxygen partial pressure[137,150,151] or an electric field[152] is highly advantageous, as it allows one to isolate the origin of the volume change, of which there can be many in complex oxide materials.

Measuring the shift in the Bragg peak position can provide information on changes in the average oxygen vacancy concentration, but this approach lacks the ability to resolve vacancy distributions. For model single-crystal systems, this can be remedied by measurement and analysis of the crystal truncation rods, which represent the Fourier transform of the three-dimensional (3D) electron density of the sampled volume. Through curve fitting[153] or the use of phase retrieval methods,[154,155] one can reconstruct a 3D electron density map of the sample, much like the microscopic techniques described above. Here, the use of hard X-rays permits the *in situ* study of electron density distributions at high temperature and in varying oxygen partial pressure environments. However, large data sets need to be acquired, typically limiting the time resolution of measurements to several hours. Furthermore, these studies have high spatial resolution along the sample normal but average the electron density over the lateral dimensions of the probed volume. Therefore, high spatial resolution along the lateral dimensions requires a micro- or nanofocused beam that may be scanned across the surface. Fratini *et al.* used scanning microdiffraction to map inhomogeneities in the organization of oxygen defects

in superconducting $La_2CuO_{4+\delta}$, and this group has recently shown that the X-ray beam itself can be used to control the degree of interstitial oxygen ordering.[156,157] Focusing methods can be combined with phase retrieval techniques to image nanostructures directly both externally and internally, which is an active area of research[158] and is helping to drive the development of light sources around the globe.

X-ray scattering techniques can be indispensable when charge restructuring involves the formation of ordered structures because *in situ* X-rays can be used to observe ordering dynamically. For example, the real-time studies of $PbTiO_3$ chemical switching described above[25] showed that the reconstruction peak due to oxygen vacancy ordering appears just as the $PbTiO_3$ film switches to the negative polarization state. Similarly, *in situ* X-ray studies of oxygen adsorption on Cu(001) surfaces found that oxygen ordering takes place (forming a $c(2 \times 2)$-O adlayer) as soon as a half monolayer of oxygen is adsorbed onto the surface.[159] Such measurements, however, depend on the exact scattering conditions. For instance, the adsorption of oxygen on top of the Pb atoms in the $PbTiO_3$ surface, as in Figure 2a, would result in negligible changes in the scattering.

Another *in situ* X-ray approach is to use spectroscopic methods, such as X-ray absorption spectroscopy carried out at either the oxygen or a cation absorption edge. For materials with a multivalent cation like $SrCoO_{3-\delta}$, X-ray absorption near-edge structure (XANES) measurements of the cobalt edge can be used to determine oxygen vacancy concentrations.[160,161] Such measurements of the cation K-edge can be conducted *in situ* with varying oxygen partial pressure.[161] The effect of oxygen nonstoichiometry can also be found at the oxygen K-edge,[160] but here, the low X-ray energy typically prohibits ambient pressures and *in situ* investigations. A nice example of the power of modern spectroscopic techniques was demonstrated by Lenser *et al.*,[162] who recently used a microfocused beam to map Fe XANES spectra through the electrode of a resistively switched Fe-doped $SrTiO_3$ epitaxial film. This allowed them to determine the location and approximate size of the main conducting filament, which was composed of Fe oxygen vacancy defects.

The spectra of low-*Z* elements can also be investigated with inelastic X-ray scattering (IXS) techniques.[163,164] Since inelastic processes can probed using hard X-rays, this permits the examination of elements with sub-keV binding energies even in high-pressure environments. Fister *et al.*[165] have recently extended the technique to demonstrate high surface sensitivity using grazing incidence angles. This allowed them to distinguish the oxygen K-edge spectrum from a 10 nm thick $La_{0.6}Sr_{0.4}CoO_3$ film *versus* that from the underlying $SrTiO_3$ substrate. However, quantitative extraction of oxygen vacancy concentrations remains difficult. As noted above, this issue can be addressed through the ongoing efforts to incorporate larger defect structures into *ab initio* computational theory.

SUMMARY AND PROSPECTS

In this Perspective, we aimed to provide a (necessarily brief) overview of the roles of vacancies and electrochemistry on physical studies. While a number of studies in disparate areas of physics have elucidated the role of surface electrochemistry in physical systems, a much larger body of work ignores the possibility of electrochemical processes and assumes constant (and often even ideal) stoichiometries. While generally the case for bulk systems, nanoscale systems, whether surfaces, interfaces, or tunneling barriers, can often exhibit electrochemical responses that dominate relatively weak physical coupling mechanisms.

The systematic exploration of these phenomena requires instrumental, theoretical, and conceptual developments. From the instrumental perspective, SPM, scattering techniques, and electron microscopy all can provide information relevant to vacancy dynamics. However, the separation of electrochemical and physical responses is possible if the chemical degrees of freedom can be controlled and varied during experiment. This separation requires *in situ* studies, in which electrochemical potentials of mobile species are defined and surfaces are in dynamic equilibrium with the environment, rather than relying on the kinetic stabilities of materials. From the theoretical perspective, mesoscopic and atomistic theories integrating physical and electrochemical degrees of freedom are required.

Perhaps most important is the role of conceptual understanding. The transition to nanometer scales blurs the boundaries between classical, physical, and electrochemical phenomena, due to smaller transport lengths, larger chemical and electrostatic potential gradients, and higher surface/volume ratios. Whenever a new and exciting physical behavior is observed, perhaps the question should be—which aspects are due to physics and which to electrochemistry? Gaining this knowledge will provide new and powerful ways to control and to tailor materials at the nanoscale.

Conflict of Interest: The authors declare no competing financial interest.

Acknowledgment. This research was conducted in part (S.V.K.) at the Center for Nanophase Materials Sciences, which is sponsored at Oak Ridge National Laboratory by the Scientific User Facilities Division, Office of Basic Energy Sciences, U.S. Department of Energy. A.B. and D.D.F. were supported by the U.S. Department of Energy, Office of Basic Energy Sciences (BES), Materials Sciences and Engineering Division. The authors gratefully acknowledge discussions with multiple colleagues, comments by A. Tagantsev (EPFL) and P. Littlewood (ANL), and images by Stephen Jesse and Zheng Gai (ORNL).

REFERENCES AND NOTES

1. Waser, R., Ed. *Nanoelectronics and Information Technology*, 3rd ed.; Wiley-VCH: Weinheim, Germany, 2012.
2. Loss, D.; DiVincenzo, D. P. Quantum Computation with Quantum Dots. *Phys. Rev. A* **1998**, *57*, 120–126.

3. Braunstein, S. L.; Kimble, H. J. Teleportation of Continuous Quantum Variables. *Phys. Rev. Lett.* **1998**, *80*, 869–872.
4. Wolf, S. A.; Awschalom, D. D.; Buhrman, R. A.; Daughton, J. M.; von Molnar, S.; Roukes, M. L.; Chtchelkanova, A. Y.; Treger, D. M. Spintronics: A Spin-Based Electronics Vision for the Future. *Science* **2001**, *294*, 1488–1495.
5. Zutic, I.; Fabian, J.; Das Sarma, S. Spintronics: Fundamentals and Applications. *Rev. Mod. Phys.* **2004**, *76*, 323–410.
6. Binder, K.; Young, A. P. Spin-Glasses—Experimental Facts, Theoretical Concepts, and Open Questions. *Rev. Mod. Phys.* **1986**, *58*, 801–976.
7. Gerber, C.; Lang, H. P. How the Doors to the Nanoworld Were Opened. *Nat. Nanotechnol.* **2006**, *1*, 3–5.
8. http://www.nano.gov.
9. Imada, M.; Fujimori, A.; Tokura, Y. Metal-Insulator Transitions. *Rev. Mod. Phys.* **1998**, *70*, 1039–1263.
10. Dagotto, E. Complexity in Strongly Correlated Electronic Systems. *Science* **2005**, *309*, 257–262.
11. Adler, S. B. Factors Governing Oxygen Reduction in Solid Oxide Fuel Cell Cathodes. *Chem. Rev.* **2004**, *104*, 4791–4843.
12. Minh, N. Q. Ceramic Fuel-Cells. *J. Am. Ceram. Soc.* **1993**, *76*, 563–588.
13. Bagotsky, V. S. *Fuel Cells: Problems and Solutions*; Wiley: Hoboken, NJ, 2009.
14. Lankhorst, M. H. R.; Bouwmeester, H. J. M.; Verweij, H. Use of the Rigid Band Formalism To Interpret the Relationship between O Chemical Potential and Electron Concentration in La1-Xsrxcoo3-Delta. *Phys. Rev. Lett.* **1996**, *77*, 2989–2992.
15. Mizusaki, J.; Mori, N.; Takai, H.; Yonemura, Y.; Minamiue, H.; Tagawa, H.; Dokiya, M.; Inaba, H.; Naraya, K.; Sasamoto, T.; *et al.* Oxygen Nonstoichiometry and Defect Equilibrium in the Perovskite-Type Oxides $La_{1-x}Sr_xMnO_{3+\partial}$. *Solid State Ionics* **2000**, *129*, 163–177.
16. Mitchell, J. F.; Argyriou, D. N.; Potter, C. D.; Hinks, D. G.; Jorgensen, J. D.; Bader, S. D. Structural Phase Diagram of $La_{1-x}Sr_xMnO_{3+\partial}$: Relationship to Magnetic and Transport Properties. *Phys. Rev. B* **1996**, *54*, 6172–6183.
17. Jorgensen, J.; Dabrowski, B.; Pei, S.; Hinks, D. G.; Soderholm, L.; Morosin, B.; Schirber, J. E.; Venturini, E. L.; Ginley, D. S. Superconducting Phase of $La_2CuO_{4+\delta}$: A Superconducting Composition Resulting from Phase Separation. *Phys. Rev. B* **1988**, *38*, 11337–11345.
18. Spaldin, N. A.; Fiebig, M. The Renaissance of Magnetoelectric Multiferroics. *Science* **2005**, *309*, 391–392.
19. Jesse, S.; Kumar, A.; Arruda, T. M.; Kim, Y.; Kalinin, S. V.; Ciucci, F. Electrochemical Strain Microscopy: Probing Ionic and Electrochemical Phenomena in Solids at the Nanometer Level. *MRS Bull.* **2012**, *37*, 651–658.
20. Tagantsev, A. K.; Cross, L. E.; Fousek, J. *Domains in Ferroic Crystals and Thin Films*; Springer: New York, 2010.
21. Fridkin, V. M. *Ferroelectric Semiconductors*; Springer: New York, 1980.
22. Kalinin, S. V.; Bonnell, D. A. Screening Phenomena on Oxide Surfaces and Its Implications for Local Electrostatic and Transport Measurements. *Nano Lett.* **2004**, *4*, 555–560.
23. Kalinin, S. V.; Bonnell, D. A. Effect of Phase Transition on the Surface Potential of the $BaTiO_3$(100) Surface by Variable Temperature Scanning Surface Potential Microscopy. *J. Appl. Phys.* **2000**, *87*, 3950–3957.
24. Cunningham, S.; Larkin, I. A.; Davis, J. H. Noncontact Scanning Probe Microscope Potentiometry of Surface Charge Patches: Origin and Interpretation of Time-Dependent Signals. *Appl. Phys. Lett.* **1998**, *73*, 123–125.
25. Wang, R. V.; Fong, D. D.; Jiang, F.; Highland, M. J.; Fuoss, P. H.; Thompson, C.; Kolpak, A. M.; Eastman, J. A.; Streiffer, S. K.; Rappe, A. M.; *et al.* Reversible Chemical Switching of a Ferroelectric Film. *Phys. Rev. Lett.* **2009**, *102*, 047601.
26. Fong, D. D.; Kolpak, A. M.; Eastman, J. A.; Streiffer, S. K.; Fuoss, P. H.; Stephenson, G. B.; Thompson, C.; Kim, D. M.; Choi, K. J.; Eom, C. B.; *et al.* Stabilization of Monodomain Polarization in Ultrathin $PbTiO_3$ Films. *Phys. Rev. Lett.* **2006**, *96*, 127601.
27. Shin, J.; Nascimento, V. B.; Geneste, G.; Rundgren, J.; Plummer, E. W.; Dkhil, B.; Kalinin, S. V.; Baddorf, A. P. Atomistic Screening Mechanism of Ferroelectric Surfaces: An *In Situ* Study of the Polar Phase in Ultrathin $BaTiO_3$ Films Exposed to H_2O. *Nano Lett.* **2009**, *9*, 3720–3725.
28. Kim, Y.; Kim, J.; Buhlmann, S.; Hong, S.; Kim, Y. K.; Kim, S. H.; No, K. Screen Charge Transfer by Grounded Tip on Ferroelectric Surfaces. *Phys. Status Solidi R* **2008**, *2*, 74–76.
29. Kim, Y.; Buhlmann, S.; Hong, S.; Kim, S. H.; No, K. Injection Charge Assisted Polarization Reversal in Ferroelectric Thin Films. *Appl. Phys. Lett.* **2007**, *90*, 072910.
30. Dahan, D.; Molotskii, M.; Rosenman, G.; Rosenwaks, Y. Ferroelectric Domain Inversion: The Role of Humidity. *Appl. Phys. Lett.* **2006**, *89*, 152902.
31. Kholkin, A. L.; Bdikin, I. K.; Shvartsman, V. V.; Pertsev, N. A. Anomalous Polarization Inversion in Ferroelectrics *via* Scanning Force Microscopy. *Nanotechnology* **2007**, *18*, 095502.
32. Buhlmann, S.; Colla, E.; Muralt, P. Polarization Reversal Due to Charge Injection in Ferroelectric Films. *Phys. Rev. B* **2005**, *72*, 214120.
33. Streiffer, S. K.; Eastman, J. A.; Fong, D. D.; Thompson, C.; Munkholm, A.; Murty, M. V. R.; Auciello, O.; Bai, G. R.; Stephenson, G. B. Observation of Nanoscale 180° Stripe Domains in Ferroelectric $PbTiO_3$ Thin Films. *Phys. Rev. Lett.* **2002**, *89*, 067601.
34. Highland, M. J.; Fister, T. T.; Fong, D. D.; Fuoss, P. H.; Thompson, C.; Eastman, J. A.; Streiffer, S. K.; Stephenson, G. B. Equilibrium Polarization of Ultrathin $PbTiO_3$ with Surface Compensation Controlled by Oxygen Partial Pressure. *Phys. Rev. Lett.* **2011**, *107*, 187602.
35. Highland, M. J.; Fister, T. T.; Richard, M. I.; Fong, D. D.; Fuoss, P. H.; Thompson, C.; Eastman, J. A.; Streiffer, S. K.; Stephenson, G. B. Polarization Switching without Domain Formation at the Intrinsic Coercive Field in Ultrathin Ferroelectric $PbTiO_3$. *Phys. Rev. Lett.* **2010**, *105*, 167601.
36. Stephenson, G. B.; Highland, M. J. Equilibrium and Stability of Polarization in Ultrathin Ferroelectric Films with Ionic Surface Compensation. *Phys. Rev. B* **2011**, *84*, 064107.
37. Kalinin, S. V.; Bonnell, D. A. Characterization of Ferroelectric $BaTiO_3$-(100) Surfaces by Variable Temperature Scanning Surface Potential Microscopy and Piezoresponse Imaging. In *Ferroelectric Thin Films VIII*; Schwartz, R. W., McIntyre, P. C., Miyasaka, Y., Summerfelt, S. R., Wouters, D., Eds.; Materials Research Society: Warrendale, PA, 2000; Vol. 596, pp 327−332.
38. Kalinin, S. V.; Bonnell, D. A. Local Potential and Polarization Screening on Ferroelectric Surfaces. *Phys. Rev. B* **2001**, *63*, 125411.
39. Kalinin, S. V.; Johnson, C. Y.; Bonnell, D. A. Domain Polarity and Temperature Induced Potential Inversion on the $BaTiO_3$(100) Surface. *J. Appl. Phys.* **2002**, *91*, 3816–3823.
40. Kalinin, S. V.; Bonnell, D. A. Surface Potential at Surface−Interface Junctions in $SrTiO_3$ Bicrystals. *Phys. Rev. B* **2000**, *62*, 10419–10430.
41. Kalinin, S. V.; Shin, J.; Jesse, S.; Geohegan, D.; Baddorf, A. P.; Lilach, Y.; Moskovits, M.; Kolmakov, A. Electronic Transport Imaging in a Multiwire SnO_2 Chemical Field-Effect Transistor Device. *J. Appl. Phys.* **2005**, *98*, 044503.
42. Rodriguez, B. J.; Nemanich, R. J.; Kingon, A.; Gruverman, A.; Kalinin, S. V.; Terabe, K.; Liu, X. Y.; Kitamura, K. Domain Growth Kinetics in Lithium Niobate Single Crystals Studied by Piezoresponse Force Microscopy. *Appl. Phys. Lett.* **2005**, *86*, 012906.

43. Tybell, T.; Paruch, P.; Giamarchi, T.; Triscone, J. M. Domain Wall Creep in Epitaxial Ferroelectric Pb($Zr_{0.2}Ti_{0.8}$)O_3 Thin Films. *Phys. Rev. Lett.* **2002**, *89*, 097601.
44. He, D. Y.; Qiao, L. J.; Volinsky, A. A. Humidity Effect on $BaTiO_3$ C-Domain Surface Potential Inversion Induced by Electric Field. *J. Appl. Phys.* **2011**, *110*, 074104.
45. Morozovska, A. N.; Svechnikov, S. V.; Eliseev, E. A.; Jesse, S.; Rodriguez, B. J.; Kalinin, S. V. Piezoresponse Force Spectroscopy of Ferroelectric-Semiconductor Materials. *J. Appl. Phys.* **2007**, *102*, 114108.
46. Ohtomo, A.; Muller, D. A.; Grazul, J. L.; Hwang, H. Y. Artificial Charge-Modulation in Atomic-Scale Perovskite Titanate Superlattices. *Nature* **2002**, *419*, 378–380.
47. Willmott, P. R.; Pauli, S. A.; Herger, R.; Schleputz, C. M.; Martoccia, D.; Patterson, B. D.; Delley, B.; Clarke, R.; Kumah, D.; Cionca, C.; *et al.* Structural Basis for the Conducting Interface between $LaAlO_3$ and $SrTiO_3$. *Phys. Rev. Lett.* **2007**, *99*, 155502.
48. Qiao, L.; Droubay, T. C.; Kaspar, T. C.; Sushko, P. V.; Chambers, S. A. Cation Mixing, Band Offsets and Electric Fields at $LaAlO_3$/$SrTiO_3$(001) Heterojunctions with Variable La:Al Atom Ratio. *Surf. Sci.* **2011**, *605*, 1381–1387.
49. Chambers, S. A.; Engelhard, M. H.; Shutthanandan, V.; Zhu, Z.; Droubay, T. C.; Qiao, L.; Sushko, P. V.; Feng, T.; Lee, H. D.; Gustafsson, T.; *et al.* Instability, Intermixing and Electronic Structure at the Epitaxial $LaAlO_3$/$SrTiO_3$(001) Heterojunction. *Surf. Sci. Rep.* **2010**, *65*, 317–352.
50. Zhong, Z. C.; Xu, P. X.; Kelly, P. J. Polarity-Induced Oxygen Vacancies at $LaAlO_3$/$SrTiO_3$ Interfaces. *Phys. Rev. B* **2010**, *82*, 165127.
51. Zhang, L. X.; Zhou, X. F.; Wang, H. T.; Xu, J. J.; Li, J. B.; Wang, E. G.; Wei, S. H. Origin of Insulating Behavior of the p-Type $LaAlO_3$/$SrTiO_3$ Interface: Polarization-Induced Asymmetric Distribution of Oxygen Vacancies. *Phys. Rev. B* **2010**, *82*, 125412.
52. Herranz, G.; Basletic, M.; Bibes, M.; Carretero, C.; Tafra, E.; Jacquet, E.; Bouzehouane, K.; Deranlot, C.; Hamzic, A.; Broto, J. M.; *et al.* High Mobility in $LaAlO_3$/$SrTiO_3$ Heterostructures: Origin, Dimensionality, and Perspectives. *Phys. Rev. Lett.* **2007**, *98*, 216803.
53. Siemons, W.; Koster, G.; Yamamoto, H.; Harrison, W. A.; Lucovsky, G.; Geballe, T. H.; Blank, D. H. A.; Beasley, M. R. Origin of Charge Density at $LaAlO_3$ on $SrTiO_3$ Heterointerfaces: Possibility of Intrinsic Doping. *Phys. Rev. Lett.* **2007**, *98*, 196802.
54. Kalabukhov, A.; Gunnarsson, R.; Borjesson, J.; Olsson, E.; Claeson, T.; Winkler, D. Effect of Oxygen Vacancies in the $SrTiO_3$ Substrate on the Electrical Properties of the $LaAlO_3$/$SrTiO_3$ Interface. *Phys. Rev. B* **2007**, *75*, 121404.
55. Xie, Y. W.; Hikita, Y.; Bell, C.; Hwang, H. Y. Control of Electronic Conduction at an Oxide Heterointerface Using Surface Polar Adsorbates. *Nat. Commun.* **2011**, *2*, 494.
56. Xie, Y. W.; Bell, C.; Hikita, Y.; Hwang, H. Y. Tuning the Electron Gas at an Oxide Heterointerface *via* Free Surface Charges. *Adv. Mater.* **2011**, *23*, 1744–1747.
57. Xie, Y. W.; Bell, C.; Yajima, T.; Hikita, Y.; Hwang, H. Y. Charge Writing at the $LaAlO_3$/$SrTiO_3$ Surface. *Nano Lett.* **2010**, *10*, 2588–2591.
58. Bi, F.; Bogorin, D. F.; Cen, C.; Bark, C. W.; Park, J. W.; Eom, C. B.; Levy, J. "Water-Cycle" Mechanism for Writing and Erasing Nanostructures at the $LaAlO_3$/$SrTiO_3$ Interface. *Appl. Phys. Lett.* **2010**, *97*, 173110.
59. Cheng, G. L.; Siles, P. F.; Bi, F.; Cen, C.; Bogorin, D. F.; Bark, C. W.; Folkman, C. M.; Park, J. W.; Eom, C. B.; Medeiros-Ribeiro, G.; *et al.* Sketched Oxide Single-Electron Transistor. *Nat. Nanotechnol.* **2011**, *6*, 343–347.
60. Bi, F.; Bogorin, D. F.; Cen, C.; Bark, C. W.; Park, J. W.; Eom, C. B.; Levy, J. "Water-Cycle" Mechanism for Writing and Erasing Nanostructures at the $LaAlO_3$/$SrTiO_3$ Interface (Vol 97, 173110, 2010). *Appl. Phys. Lett.* **2012**, *100*, 199901.
61. Bristowe, N. C.; Littlewood, P. B.; Artacho, E. Surface Defects and Conduction in Polar Oxide Heterostructures. *Phys. Rev. B* **2011**, *83*, 205405.
62. Scott, J. F.; Dawber, M. Oxygen-Vacancy Ordering as a Fatigue Mechanism in Perovskite Ferroelectrics. *Appl. Phys. Lett.* **2000**, *76*, 3801–3803.
63. Tagantsev, A. K.; Stolichnov, I.; Colla, E. L.; Setter, N. Polarization Fatigue in Ferroelectric Films: Basic Experimental Findings, Phenomenological Scenarios, and Microscopic Features. *J. Appl. Phys.* **2001**, 1387–1402.
64. Strukov, D. B.; Snider, G. S.; Stewart, D. R.; Williams, R. S. The Missing Memristor Found. *Nature* **2008**, *453*, 80–83.
65. Szot, K.; Rogala, M.; Speier, W.; Klusek, Z.; Besmehn, A.; Waser, R. TiO_2—A Prototypical Memristive Material. *Nanotechnology* **2011**, *22*, 254001.
66. Waser, R.; Dittmann, R.; Staikov, G.; Szot, K. Redox-Based Resistive Switching Memories—Nanoionic Mechanisms, Prospects, and Challenges. *Adv. Mater.* **2009**, *21*, 2632–2663.
67. Valov, I.; Waser, R.; Jameson, J. R.; Kozicki, M. N. Electrochemical Metallization Memories—Fundamentals, Applications, Prospects. *Nanotechnology* **2011**, *22*, 254003.
68. Waser, R.; Aono, M. Nanoionics-Based Resistive Switching Memories. *Nat. Mater.* **2007**, *6*, 833–840.
69. Jiang, W.; Noman, M.; Lu, Y. M.; Bain, J. A.; Salvador, P. A.; Skowronski, M. Mobility of Oxygen Vacancy in $SrTiO_3$ and Its Implications for Oxygen-Migration-Based Resistance Switching. *J. Appl. Phys.* **2011**, *110*, 034509.
70. Yi, H. T.; Choi, T.; Choi, S. G.; Oh, Y. S.; Cheong, S. W. Mechanism of the Switchable Photovoltaic Effect in Ferroelectric $BiFeO_3$. *Adv. Mater.* **2011**, *23*, 3403–3407.
71. Borisevich, A. Y.; Morozovska, A. N.; Kim, Y. M.; Leonard, D.; Oxley, M. P.; Biegalski, M. D.; Eliseev, E. A.; Kalinin, S. V. Exploring Mesoscopic Physics of Vacancy-Ordered Systems through Atomic Scale Observations of Topological Defects. *Phys. Rev. Lett.* **2012**, *109*, 065702.
72. Goncalves-Ferreira, L.; Redfern, S. A. T.; Artacho, E.; Salje, E.; Lee, W. T. Trapping of Oxygen Vacancies in the Twin Walls of Perovskite. *Phys. Rev. B* **2010**, *81*, 024109.
73. Calleja, M.; Dove, M. T.; Salje, E. K. H. Trapping of Oxygen Vacancies on Twin Walls of $CaTiO_3$: A Computer Simulation Study. *J. Phys.: Condens. Matter* **2003**, *15*, 2301–2307.
74. Seidel, J.; Martin, L. W.; He, Q.; Zhan, Q.; Chu, Y. H.; Rother, A.; Hawkridge, M. E.; Maksymovych, P.; Yu, P.; Gajek, M.; *et al.* Conduction at Domain Walls in Oxide Multiferroics. *Nat. Mater.* **2009**, *8*, 229–234.
75. Lubk, A.; Gemming, S.; Spaldin, N. A. First-Principles Study of Ferroelectric Domain Walls in Multiferroic Bismuth Ferrite. *Phys. Rev. B* **2009**, *80*, 104110.
76. Gureev, M. Y.; Tagantsev, A. K.; Setter, N. Head-to-Head and Tail-to-Tail 180 Degrees Domain Walls in an Isolated Ferroelectric. *Phys. Rev. B* **2011**, *83*, 184104.
77. Eliseev, E. A.; Morozovska, A. N.; Svechnikov, G. S.; Maksymovych, P.; Kalinin, S. V. Domain Wall Conduction in Multiaxial Ferroelectrics. *Phys. Rev. B* **2012**, *85*, 045312.
78. Eliseev, E. A.; Morozovska, A. N.; Gu, Y. J.; Borisevich, A. Y.; Chen, L. Q.; Gopalan, V.; Kalinin, S. V. Conductivity of Twin-Domain-Wall/Surface Junctions in Ferroelastics: Interplay of Deformation Potential, Octahedral Rotations, Improper Ferroelectricity, and Flexoelectric Coupling. *Phys. Rev. B* **2012**, *86*, 085416.
79. Maksymovych, P.; Morozovska, A. N.; Yu, P.; Eliseev, E. A.; Chu, Y. H.; Ramesh, R.; Baddorf, A. P.; Kalinin, S. V. Tunable Metallic Conductance in Ferroelectric Nanodomains. *Nano Lett.* **2012**, *12*, 209–213.
80. Balke, N.; Winchester, B.; Ren, W.; Chu, Y. H.; Morozovska, A. N.; Eliseev, E. A.; Huijben, M.; Vasudevan, R. K.; Maksymovych, P.; Britson, J.; *et al.* Enhanced Electric Conductivity

at Ferroelectric Vortex Cores in $BiFeO_3$. *Nat. Phys.* **2012**, *8*, 81–88.
81. Farokhipoor, S.; Noheda, B. Conduction through 71° Domain Walls in $BiFeO_3$ Thin Films. *Phys. Rev. Lett.* **2011**, *107*, 127601.
82. Guyonnet, J.; Gaponenko, I.; Gariglio, S.; Paruch, P. Conduction at Domain Walls in Insulating $Pb(Zr_{0.2}Ti_{0.8})O_3$ Thin Films. *Adv. Mater.* **2011**, *23*, 5377–5382.
83. Milne, J. S.; Rowe, A. C. H.; Arscott, S.; Renner, C. Giant Piezoresistance Effects in Silicon Nanowires and Microwires. *Phys. Rev. Lett.* **2010**, *105*, 226802.
84. Kim, W.; Javey, A.; Vermesh, O.; Wang, O.; Li, Y. M.; Dai, H. J. Hysteresis Caused by Water Molecules in Carbon Nanotube Field-Effect Transistors. *Nano Lett.* **2003**, *3*, 193–198.
85. Lee, J. S.; Ryu, S.; Yoo, K.; Choi, I. S.; Yun, W. S.; Kim, J. Origin of Gate Hysteresis in Carbon Nanotube Field-Effect Transistors. *J. Phys. Chem. C* **2007**, *111*, 12504–12507.
86. Hong, X.; Hoffman, J.; Posadas, A.; Zou, K.; Ahn, C. H.; Zhu, J. Unusual Resistance Hysteresis in N-Layer Graphene Field Effect Transistors Fabricated on Ferroelectric $Pb(Zr_{0.2}Ti_{0.8})O_3$. *Appl. Phys. Lett.* **2010**, *97*, 033114.
87. Wang, H. M.; Wu, Y. H.; Cong, C. X.; Shang, J. Z.; Yu, T. Hysteresis of Electronic Transport in Graphene Transistors. *ACS Nano* **2010**, *4*, 7221–7228.
88. Ueno, K.; Nakamura, S.; Shimotani, H.; Ohtomo, A.; Kimura, N.; Nojima, T.; Aoki, H.; Iwasa, Y.; Kawaski, M. Electric-Field-Induced Superconductivity in an Insulator. *Nat. Mater.* **2008**, *7*, 855–858.
89. Lee, Y.; Clement, C.; Hellerstedt, J.; Kinney, J.; Kinnischtzke, L.; Leng, X.; Snyder, S. D.; Goldman, A. M. Phase Diagram of Electrostatically Doped $SrTiO_3$. *Phys. Rev. Lett.* **2011**, *106*, 136809.
90. Xie, Y.; Hikita, Y.; Bell, C.; Hwang, H. Y. Control of Electronic Conduction at an Oxide Heterointerface Using Surface Polar Adsorbates. *Nat. Commun.* **2011**, *2*, 494.
91. Ho, C.; Raistrick, I. D.; Huggins, R. A. Application of Ac Techniques to the Study of Lithium Diffusion in Tungsten Trioxide Thin-Films. *J. Electrochem. Soc.* **1980**, *127*, 343–350.
92. Weppner, W.; Huggins, R. A. Electrochemical Methods for Determining Kinetic-Properties of Solids *Annu. Rev. Mater. Sci.* **1978**, *8*, 269–311.
93. Rief, M.; Oesterhelt, F.; Heymann, B.; Gaub, H. E. Single Molecule Force Spectroscopy on Polysaccharides by Atomic Force Microscopy. *Science* **1997**, *275*, 1295–1297.
94. Bonnell, D. A.; Kalinin, S. V.; Kholkin, A. L.; Gruverman, A. Piezoresponse Force Microscopy: A Window into Electromechanical Behavior at the Nanoscale. *MRS Bull.* **2009**, *34*, 648–657.
95. Gruverman, A.; Kholkin, A. Nanoscale Ferroelectrics: Processing, Characterization and Future Trends. *Rep. Prog. Phys.* **2006**, *69*, 2443–2474.
96. Kalinin, S. V.; Morozovska, A. N.; Chen, L. Q.; Rodriguez, B. J. Local Polarization Dynamics in Ferroelectric Materials. *Rep. Prog. Phys.* **2010**, *73*, 056502.
97. Oliver, W. C.; Pharr, G. M. An Improved Technique for Determining Hardness and Elastic-Modulus Using Load and Displacement Sensing Indentation Experiments. *J. Mater. Res.* **1992**, *7*, 1564–1583.
98. Fuchigami, K.; Gai, Z.; Ward, T. Z.; Yin, L. F.; Snijders, P. C.; Plummer, E. W.; Shen, J. Tunable Metallicity of the $La_{5/8}Ca_{3/8}MnO_3(001)$ Surface by an Oxygen Overlayer. *Phys. Rev. Lett.* **2009**, *102*, 066104.
99. Lu, H.; Bark, C. W.; de los Ojos, D. E.; Alcala, J.; Eom, C. B.; Catalan, G.; Gruverman, A. Mechanical Writing of Ferroelectric Polarization. *Science* **2012**, *336*, 59–61.
100. Shin, J.; Borisevich, A. Y.; Meunier, V.; Zhou, J.; Plummer, E. W.; Kalinin, S. V.; Baddorf, A. P. Oxygen-Induced Surface Reconstruction of $SrRuO_3$ and Its Effect on the $BaTiO_3$ Interface. *ACS Nano* **2010**, *4*, 4190–4196.
101. Forster, S.; Huth, M.; Schindler, K. M.; Widdra, W. Epitaxial $BaTiO_3$-(100) Films on Pt(100): A Low-Energy Electron Diffraction, Scanning Tunneling Microscopy, and X-ray Photoelectron Spectroscopy Study. *J. Chem. Phys.* **2011**, *135*, 104701.
102. Hagendorf, C.; Shantyr, R.; Neddermeyer, H.; Widdra, W. Pressure-Dependent Ni-O Phase Transitions and Ni Oxide Formation on Pt(111): An *In Situ* STM Study at Elevated Temperatures. *Phys. Chem. Chem. Phys.* **2006**, *8*, 1575–1583.
103. Balke, N.; Jesse, S.; Morozovska, A. N.; Eliseev, E.; Chung, D. W.; Kim, Y.; Adamczyk, L.; Garcia, R. E.; Dudney, N.; Kalinin, S. V. Nanoscale Mapping of Ion Diffusion in a Lithium-Ion Battery Cathode. *Nat. Nanotechnol.* **2010**, *5*, 749–754.
104. Balke, N.; Jesse, S.; Kim, Y.; Adamczyk, L.; Ivanov, I. N.; Dudney, N. J.; Kalinin, S. V. Decoupling Electrochemical Reaction and Diffusion Processes in Ionically-Conductive Solids on the Nanometer Scale. *ACS Nano* **2010**, *4*, 7349–7357.
105. Kumar, A.; Ciucci, F.; Morozovska, A. N.; Kalinin, S. V.; Jesse, S. Measuring Oxygen Reduction/Evolution Reactions on the Nanoscale. *Nat. Chem.* **2011**, *3*, 707–713.
106. Morozovska, A. N.; Eliseev, E. A.; Balke, N.; Kalinin, S. V. Local Probing of Ionic Diffusion by Electrochemical Strain Microscopy: Spatial Resolution and Signal Formation Mechanisms. *J. Appl. Phys.* **2010**, *108*, 053712.
107. Morozovska, A. N.; Eliseev, E. A.; Kalinin, S. V. Electromechanical Probing of Ionic Currents in Energy Storage Materials. *Appl. Phys. Lett.* **2010**, *96*, 222906.
108. Krivanek, O. L.; Chisholm, M. F.; Nicolosi, V.; Pennycook, T. J.; Corbin, G. J.; Dellby, N.; Murfitt, M. F.; Own, C. S.; Szilagyi, Z. S.; Oxley, M. P.; *et al.* Atom-by-Atom Structural and Chemical Analysis by Annular Dark-Field Electron Microscopy. *Nature* **2010**, *464*, 571–574.
109. Varela, M.; Findlay, S. D.; Lupini, A. R.; Christen, H. M.; Borisevich, A. Y.; Dellby, N.; Krivanek, O. L.; Nellist, P. D.; Oxley, M. P.; Allen, L. J.; *et al.* Spectroscopic Imaging of Single Atoms within a Bulk Solid. *Phys. Rev. Lett.* **2004**, *92*, 095502.
110. Lovejoy, T. C.; Ramasse, Q. M.; Falke, M.; Kaeppel, A.; Terborg, R.; Zan, R.; Dellby, N.; Krivanek, O. L. Single Atom Identification by Energy Dispersive X-ray Spectroscopy. *Appl. Phys. Lett.* **2012**, *100*, 154101.
111. Varela, M.; Oxley, M. P.; Luo, W.; Tao, J.; Watanabe, M.; Lupini, A. R.; Pantelides, S. T.; Pennycook, S. J. Atomic-Resolution Imaging of Oxidation States in Manganites. *Phys. Rev. B* **2009**, *79*, 085117.
112. Tan, H.; Turner, S.; Yücelen, E.; Verbeeck, J.; Van Tendeloo, G. 2D Atomic Mapping of Oxidation States in Transition Metal Oxides by Scanning Transmission Electron Microscopy and Electron Energy-Loss Spectroscopy. *Phys. Rev. Lett.* **2011**, *107*, 107602.
113. Haruta, M.; Kurata, H.; Komatsu, H.; Shimakawa, Y.; Isoda, S. Site-Resolved Oxygen K-Edge Elnes of the Layered Double Perovskite La_2CuSnO_6. *Phys. Rev. B* **2009**, *80*, 165123.
114. Turner, S.; Verbeeck, J.; Ramezanipour, F.; Greedan, J. E.; Van Tendeloo, G.; Botton, G. A. Atomic Resolution Coordination Mapping in Ca_2FeCoO_5 Brownmillerite by Spatially Resolved Electron Energy-Loss Spectroscopy. *Chem. Mater.* **2012**, *24*, 1904–1909.
115. Jia, C. L.; Nagarajan, V.; He, J. Q.; Houben, L.; Zhao, T.; Ramesh, R.; Urban, K.; Waser, R. Unit-Cell Scale Mapping of Ferroelectricity and Tetragonality in Epitaxial Ultrathin Ferroelectric Films. *Nat. Mater.* **2007**, *6*, 64–69.
116. Jia, C. L.; Mi, S. B.; Urban, K.; Vrejoiu, I.; Alexe, M.; Hesse, D. Atomic-Scale Study of Electric Dipoles near Charged and Uncharged Domain Walls in Ferroelectric Films. *Nat. Mater.* **2008**, *7*, 57–61.
117. Borisevich, A.; Ovchinnikov, O. S.; Chang, H. J.; Oxley, M. P.; Yu, P.; Seidel, J.; Eliseev, E. A.; Morozovska, A. N.; Ramesh, R.; Pennycook, S. J.; *et al.* Mapping Octahedral Tilts and Polarization across a Domain Wall in $BiFeO_3$ from *Z*-Contrast Scanning

Transmission Electron Microscopy Image Atomic Column Shape Analysis. *ACS Nano* **2010**, *4*, 6071–6079.

118. Jia, C. L.; Mi, S. B.; Urban, K.; Vrejoiu, I.; Alexe, M.; Hesse, D. Effect of a Single Dislocation in a Heterostructure Layer on the Local Polarization of a Ferroelectric Layer. *Phys. Rev. Lett.* **2009**, *102*, 117601.
119. Chang, H. J.; Kalinin, S. V.; Morozovska, A. N.; Huijben, M.; Chu, Y. H.; Yu, P.; Ramesh, R.; Eliseev, E. A.; Svechnikov, G. S.; Pennycook, S. J.; *et al.* Atomically Resolved Mapping of Polarization and Electric Fields across Ferroelectric/Oxide Interfaces by *Z*-Contrast Imaging. *Adv. Mater.* **2011**, *23*, 2474–2479.
120. Jia, C. L.; Urban, K. W.; Alexe, M.; Hesse, D.; Vrejoiu, I. Direct Observation of Continuous Electric Dipole Rotation in Flux-Closure Domains in Ferroelectric $Pb(Zr,Ti)O_3$. *Science* **2011**, *331*, 1420–1423.
121. Nelson, C. T.; Winchester, B.; Zhang, Y.; Kim, S. J.; Melville, A.; Adamo, C.; Folkman, C. M.; Baek, S. H.; Eom, C. B.; Schlom, D. G.; *et al.* Spontaneous Vortex Nanodomain Arrays at Ferroelectric Heterointerfaces. *Nano Lett.* **2011**, *11*, 828–834.
122. Jia, C. L.; Mi, S. B.; Faley, M.; Poppe, U.; Schubert, J.; Urban, K. Oxygen Octahedron Reconstruction in the $SrTiO_3/LaAlO_3$ Heterointerfaces Investigated Using Aberration-Corrected Ultrahigh-Resolution Transmission Electron Microscopy. *Phys. Rev. B* **2009**, *79*, 081405.
123. Borisevich, A. Y.; Chang, H. J.; Huijben, M.; Oxley, M. P.; Okamoto, S.; Niranjan, M. K.; Burton, J. D.; Tsymbal, E. Y.; Chu, Y. H.; Yu, P.; *et al.* Suppression of Octahedral Tilts and Associated Changes in Electronic Properties at Epitaxial Oxide Heterostructure Interfaces. *Phys. Rev. Lett.* **2010**, *105*, 087204.
124. Egerton, R. F. Electron Energy-Loss Spectroscopy in the TEM. *Rep. Prog. Phys.* **2009**, *72*, 016502.
125. Grunes, L. A.; Leapman, R. D.; Wilker, C. N.; Hoffmann, R.; Kunz, A. B. Oxygen-K Near-Edge Fine-Structure—An Electron-Energy-Loss Investigation with Comparisons to New Theory for Selected 3D Transition-Metal Oxides. *Phys. Rev. B* **1982**, *25*, 7157–7173.
126. Kurata, H.; Lefevre, E.; Colliex, C.; Brydson, R. Electron-Energy-Loss Near-Edge Structures in the Oxygen K-Edge Spectra of Transition-Metal Oxides. *Phys. Rev. B* **1993**, *47*, 13763–13768.
127. Luo, W. D.; Varela, M.; Tao, J.; Pennycook, S. J.; Pantelides, S. T. Electronic and Crystal-Field Effects in the Fine Structure of Electron Energy-Loss Spectra of Manganites. *Phys. Rev. B* **2009**, *79*, 052405.
128. Cantoni, C.; Gao, Y.; Wee, S. H.; Specht, E. D.; Gazquez, J.; Meng, J.; Pennycook, S. J.; Goyal, A. Strain-Driven Oxygen Deficiency in Self-Assembled, Nanostructured, Composite Oxide Films. *ACS Nano* **2011**, *5*, 4783–4789.
129. Jia, C. L.; Lentzen, M.; Urban, K. Atomic-Resolution Imaging of Oxygen in Perovskite Ceramics. *Science* **2003**, *299*, 870–873.
130. Muller, D. A.; Nakagawa, N.; Ohtomo, A.; Grazul, J. L.; Hwang, H. Y. Atomic-Scale Imaging of Nanoengineered Oxygen Vacancy Profiles in $SrTiO_3$. *Nature* **2004**, *430*, 657–661.
131. Bertaut, E. F.; Blum, P.; Sagnieres, A. Structure du Ferrite Bicalcique et de la Brownmillerite. *Acta Crystallogr.* **1959**, *12*, 149–159.
132. Gazquez, J.; Luo, W.; Oxley, M. P.; Prange, M.; Torija, M. A.; Sharma, M.; Leighton, C.; Pantelides, S. T.; Pennycook, S. J.; Varela, M. Atomic-Resolution Imaging of Spin-State Superlattices in Nanopockets within Cobaltite Thin Films. *Nano Lett.* **2011**, *11*, 973–976.
133. Ito, Y.; Klie, R. F.; Browning, N. S. Atomic Resolution Analysis of the Defect Chemistry and Microdomain Structure of Brownmillerite-Type Strontium Cobaltite. *J. Am. Ceram. Soc.* **2002**, *85*, 969–976.
134. Klenov, D. O.; Donner, W.; Foran, B.; Stemmer, S. Impact of Stress on Oxygen Vacancy Ordering in Epitaxial $(La_{0.5}Sr_{0.5})CoO_{3-\partial}$ Thin Films. *Appl. Phys. Lett.* **2003**, *82*, 3427–3429.
135. Klie, R. F.; Ito, Y.; Stemmer, S.; Browning, N. S. Observation of Oxygen Vacancy Ordering and Segregation in Perovskite Oxides. *Ultramicroscopy* **2001**, *86*, 289–302.
136. Stemmer, S.; Jacobson, A. J.; Chen, X.; Ignatiev, A. Oxygen Vacancy Ordering in Epitaxial $La_{0.5}Sr_{0.5}CoO_{3-\partial}$ Thin Films on (001) $LaAlO_3$. *J. Appl. Phys.* **2001**, *90*, 3319–3324.
137. Chen, X. Y.; Yu, J. S.; Adler, S. B. Thermal and Chemical Expansion of Sr-Doped Lanthanum Cobalt Oxide $(La_{1-x}Sr_xCoO_{3-\partial})$. *Chem. Mater.* **2005**, *17*, 4537–4546.
138. Adler, S. B. Chemical Expansivity of Electrochemical Ceramics. *J. Am. Ceram. Soc.* **2001**, *84*, 2117–2119.
139. Tsipis, E. V.; Naumovich, E. N.; Patrakeev, M. V.; Yaremchenko, A. A.; Marozau, I. P.; Kovalevsky, A. V.; Waerenborgh, J. C.; Kharton, V. V. Oxygen Deficiency, Vacancy Clustering and Ionic Transport in $(La,Sr)CoO_{3-\partial}$. *Solid State Ionics* **2011**, *192*, 42–48.
140. Chen, X. Y.; Yu, J. S.; Adler, S. B. Thermal and Chemical Expansion of Sr-Doped Lanthanum Cobalt Oxide $(La_{1-x}Sr_xCoO_{3-\partial})$. *Chem. Mater.* **2005**, *17*, 4537–4546.
141. Kim, Y.-M.; He, J.; Biegalski, M. D.; Ambaye, H.; Lauter, V.; Christen, H. M.; Pantelides, S. T.; Pennycook, S. J.; Kalinin, S. V.; Borisevich, A. Y. Probing Oxygen Vacancy Concentration and Homogeneity in Solid-Oxide Fuel-Cell Cathode Materials on the Subunit-Cell Level. *Nat. Mater.* **2012**, *11*, 888–894.
142. Glazer, A. M. Classification of Tilted Octahedra in Perovskites. *Acta Crystallogr., B* **1972**, *28*, 3384–3392.
143. Borisevich, A. Y.; Lupini, A. R.; He, J.; Eliseev, E. A.; Morozovska, A. N.; Svechnikov, G. S.; Yu, P.; Chu, Y. H.; Ramesh, R.; Pantelides, S. T.; *et al.* Direct Observation of an Interface Dipole between Two Metallic Oxides Caused by Localized Oxygen Vacancies. *Phys. Rev. B* **2012**, *86*, 140102.
144. Chisholm, M. F.; Luo, W. D.; Oxley, M. P.; Pantelides, S. T.; Lee, H. N. Atomic-Scale Compensation Phenomena at Polar Interfaces. *Phys. Rev. Lett.* **2010**, *105*, 197602.
145. Cantoni, C.; Gazquez, J.; Miletto Granozio, F.; Oxley, M. P.; Varela, M.; Lupini, A. R.; Pennycook, S. J.; Aruta, C.; di Uccio, U. S.; Perna, P.; *et al.* Electron Transfer and Ionic Displacements at the Origin of the 2D Electron Gas at the LAO/STO Interface: Direct Measurements with Atomic-Column Spatial Resolution. *Adv. Mater.* **2012**, *24*, 3952–3957.
146. Freedman, D. A.; Roundy, D.; Arias, T. A. Elastic Effects of Vacancies in Strontium Titanate: Short- and Long-Range Strain Fields, Elastic Dipole Tensors, and Chemical Strain. *Phys. Rev. B* **2009**, *80*, 064108.
147. Kim, Y.; Disa, A. S.; Babakol, T. E.; Brock, J. D. Strain Screening by Mobile Oxygen Vacancies in $SrTiO_3$. *Appl. Phys. Lett.* **2010**, *96*, 251901.
148. Donner, W.; Chen, C.; Liu, M.; Jacobson, A. J.; Lee, Y.-L.; Gadre, M.; Morgan, D. Epitaxial Strain-Induced Chemical Ordering in $La_{0.5}Sr_{0.5}CoO_{3-\partial}$ Films on $SrTiO_3$. *Chem. Mater.* **2011**, *23*, 984–988.
149. Ferguson, J. D.; Kim, Y.; Kourkoutis, L. F.; Vodnick, A.; Woll, A. R.; Muller, D. A.; Brock, J. D. Epitaxial Oxygen Getter for a Brownmillerite Phase Transformation in Manganite Films. *Adv. Mater.* **2011**, *23*, 1226–1230.
150. Bishop, S. R.; Duncan, K. L.; Wachsman, E. D. Surface and Bulk Defect Equilibria in Strontium-Doped Lanthanum Cobalt Iron Oxide. *J. Electrochem. Soc.* **2009**, *156*, B1242–B1248.
151. Miyoshi, S.; Kaimai, A.; Matsumoto, H.; Yashiro, K.; Nigara, Y.; Kawada, T.; Mizusaki, J. *In Situ* XRD Study on Oxygen-Excess $LaMnO_3$. *Solid State Ionics* **2004**, *175*, 383–386.
152. Ingram, B. J.; Eastman, J. A.; Chang, K. C.; Kim, S. K.; Fister, T. T.; Perret, E.; You, H.; Baldo, P. M.; Fuoss, P. H. *In Situ* X-ray Studies of Oxygen Surface Exchange Behavior in Thin Film $La_{0.6}Sr_{0.4}Co_{0.2}Fe_{0.8})_{3-\partial}$. *Appl. Phys. Lett.* **2012**, *101*, 051603.
153. Vlieg, E. Rod: A Program for Surface X-ray Crystallography. *J. Appl. Crystallogr.* **2000**, *33*, 401–405.
154. Bjorck, M.; Schleputz, C. M.; Pauli, S. A.; Martoccia, D.; Herger, R.; Willmott, P. R. Atomic Imaging of

Thin Films with Surface X-ray Diffraction: Introducing Dcaf. *J. Phys.: Condens. Matter* **2008**, *20*, 445006.
155. Yacoby, Y.; Sowwan, M.; Stern, E.; Cross, J. O.; Brewe, D.; Pindak, R.; Pitney, J.; Dufresne, E. M.; Clarke, R. Direct Determination of Epitaxial Interface Structure in Gd_2O_3 Passivation of GaAs. *Nat. Mater.* **2002**, *1*, 99–101.
156. Fratini, M.; Poccia, N.; Ricci, A.; Campi, G.; Burghammer, M.; Aeppli, G.; Bianconi, A. Scale-Free Structural Organization of Oxygen Interstitials in La_2CuO_{4+y}. *Nature* **2010**, *466*, 841–844.
157. Poccia, N.; Fratini, M.; Ricci, A.; Campi, G.; Barba, L.; Vittorini-Orgeas, A.; Bianconi, G.; Aeppli, G.; Bianconi, A. Evolution and Control of Oxygen Order in a Cuprate Superconductor. *Nat. Mater.* **2011**, *10*, 733–736.
158. Hruszkewycz, S. O.; Folkman, C. M.; Highland, M. J.; Holt, M. V.; Baek, S. H.; Streiffer, S. K.; Baldo, P.; Eom, C. B.; Fuoss, P. H. X-ray Nanodiffraction of Tilted Domains in a Poled Epitaxial $BiFeO_3$ Thin Film. *Appl. Phys. Lett.* **2011**, *99*, 232903.
159. Iddir, H.; Fong, D. D.; Zapol, P.; Fuoss, P. H.; Curtiss, L. A.; Zhou, G. W.; Eastman, J. A. Order-Disorder Phase Transition of the Cu(001) Surface under Equilibrium Oxygen Pressure. *Phys. Rev. B* **2007**, *76*, 241404.
160. Karvonen, L.; Valkeapaa, M.; Liu, R. S.; Chen, J. M.; Yamauchi, H.; Karppinen, M. O-*K* and Co-*L* XANES Study on Oxygen Intercalation in Perovskite $SrCoO_{3-\partial}$. *Chem. Mater.* **2010**, *22*, 70–76.
161. Le Toquin, R.; Paulus, W.; Cousson, A.; Prestipino, C.; Lamberti, C. Time-Resolved *In Situ* Studies of Oxygen Intercalation into $SrCoO_{2.5}$, Performed by Neutron Diffraction and X-ray Absorption Spectroscopy. *J. Am. Chem. Soc.* **2006**, *128*, 13161–13174.
162. Lenser, C.; Kuzmin, A.; Purans, J.; Kalinko, A.; Waser, R.; Dittmann, R. Probing the Oxygen Vacancy Distribution in Resistive Switching Fe-$SrTiO_3$ Metal-Insulator-Metal-Structures by Micro-X-ray Absorption Near-Edge Structure. *J. Appl. Phys.* **2012**, *111*, 076101.
163. Lee, S. K.; Eng, P. J.; Mao, H.-k.; Meng, Y.; Newville, M.; Hu, M. Y.; Shu, J. Probing of Bonding Changes in B_2O_3 Glasses at High Pressure with Inelastic X-ray Scattering. *Nat. Mater.* **2005**, *4*, 851–854.
164. Mao, W. L.; Mao, H.-k.; Eng, P. J.; Trainor, T. P.; Newville, M.; Kao, C.-c.; Heinz, D. L.; Shu, J.; Meng, Y.; Hemley, R. J. Bonding Changes in Compressed Superhard Graphite. *Science* **2003**, *302*, 425–427.
165. Fister, T. T.; Fong, D. D.; Eastman, J. A.; Iddir, H.; Zapol, P.; Fuoss, P. H.; Balasubramanian, M.; Gordon, R. A.; Balasubramaniam, K. R.; Salvador, P. A. Total-Reflection Inelastic X-ray Scattering from a 10-nm Thick $La_{0.6}Sr_{0.4}CoO_3$ Thin Film. *Phys. Rev. Lett.* **2011**, *106*, 037401.